Title
How Radiation and other Forcing Factors Influence Snowmelt Runoff in Western United States

Author
Li, Chuyang

Publication Date
2022

Peer reviewed|Thesis/dissertation

UNIVERSITY OF CALIFORNIA

Los Angeles

How Radiation and other Forcing Factors Influence Snowmelt Runoff in Western United States

A thesis submitted in partial satisfaction

of the requirements for the degree Master of Arts

in Geography

by

Chuyang Li

2022

ABSTRACT OF THE THESIS

How Radiation and other Forcing Factors Influence Snowmelt Runoff in Western United States

by

Chuyang Li

Master of Arts in Geography

University of California, Los Angeles, 2022

Professor Dennis P. Lettenmaier, Chair

This study investigates how radiation and other forcing factors, such as temperature, precipitation, and snow water equivalent (SWE) influence snowmelt runoff in 20 river basins in the Western United States. The forcing values are derived from gridded observations of precipitation and temperature, and other surface variables (such as downward solar and longwave radiation, and humidity). Using daily runoff from U.S. Geological Survey streamflow records, this paper calculated several indexes to describe the timing and magnitude of snowmelt induced spring runoff peaks and rising limb of the hydrograph. Pearson correlation coefficients is used to analyze the relationships between forcings and runoff indexes. The results show that snowmelt runoff tends to be earlier and lower at higher temperature. With higher precipitation or SWE, snowmelt runoff tends to be later and larger. For most sites, with higher net radiation,

snowmelt runoff tends to be earlier. But only for some of the sites, with higher net radiation, snowmelt runoff tends to be smaller. For other sites, the magnitude of snowmelt runoff is not correlated with net radiation.

The thesis of Chuyang Li is approved.

Yongwei Sheng

Yongkang Xue

Dennis P. Lettenmaier, Committee Chair

University of California, Los Angeles

2022

Table of Contents

List of Figures

List of Tables

1. Introduction

Snowmelt provides a crucial water resource for a large part of world's population, especially in the northern hemisphere (Mankin et al., 2015). Regions that rely on melt water from seasonal snow cover or glaciers include High Mountain Asia, Central Asia, western Russia, southern Andes, and the Western United States (Qin et al., 2020). Snowmelt in these regions is being impacted by climate change, although the direction and magnitude of changes highly depends on geographic location (Barnett et al., 2005). Particularly, in high-elevation regions like High Mountain Asia, snowpack and snowmelt changes tend to be determined by precipitation changes, while in low-elevation regions, declining snowpack and snowmelt are occurring due to warming temperatures (Adam, et al., 2008; Stewart, 2008)

Spring snowmelt plays a key role in runoff in the Western United States (Stewart, et al., 2004). Li, et al. (2017) estimate that snowmelt contributes 53% of total runoff in the region, and this number is 70% when restricted to mountainous regions. Snowmelt also contributes about 40-70% of ground water recharge in the Southwestern United States (Earman, et al., 2006). About 60 million people rely on the rivers, reservoirs, and ground water aquifers of the Western United States (Bales, et al., 2006). These water sources all depend on the contribution of snowmelt, and hence accurate prediction of snowmelt processes is the basis of water management in the region. Snowpacks also serve as reservoirs themselves, accumulating water in mountains in winter, and releasing it to drier valleys in spring and summer. In so doing, the existence of snowpacks reduces flood risk and improves water-use efficiency in the Western United States (Barnett et al., 2005). With warming climate, a larger portion of annual precipitation falls as rain rather than snow, which may result in increased of flood risk due to rain-on-snow events (Davenport, et al.,

2020; Cho, et al., 2021). On the other hand, as the climate becomes even warmer, rain-on-snow events could decrease. Earlier snowmelt also can result in a higher risk of wildfire (Westerling, et al., 2006).

Several studies have shown that the timing of spring snowmelt runoff in the Western United States, is occurring earlier (Cayan et al., 2001; Stewart, et al., 2004; Stewart, et al., 2005; McCabe & Clark, 2005; Mote, et al., 2005; Fritze, et al., 2011; Dudley, et al., 2017; Uzun, et al., 2021). Factors that determine the timing of snowmelt runoff include precipitation, SWE, temperature, wind, vapor pressure, and radiation (Zuzel & Cox, 1975). Most research agrees that winter and spring temperature is the predominating reason for the shift to earlier spring snowmelt runoff however (Cayan et al., 2001; Stewart, et al., 2005). Nonetheless, more recent research shows that in low-elevation basins, the timing of snowmelt runoff is primarily determined by melt season temperature, while in high-elevation basins, winter precipitation also plays a role (Dudley, et al., 2017).

Related to the shift in snowmelt runoff timing, the amount of snowpack (seasonal peak) is decreasing in most parts of Western United States (Hamlet, et al., 2005; Mote, et al., 2005; Mote et al., 2016). The decreasing trends in SWE (on or about April 1st, typically close to the seasonal maximum) are mostly due to a long-term increasing trend in temperature throughout the 20th Century, with precipitation variations a minor contributor (Hamlet, et al., 2005). However, at high-elevation (relatively cold stations) precipitation trends play some role (notably in the southern Sierra Nevada) (Mote et al. 2005). At low-elevation stations with relatively mild winter

temperatures SWE trends are almost entirely attributable to the increasing trend of temperature (Mote et al., 2005).

The magnitude (volume) of snowmelt runoff is also impacted by climate change. Berghuijs, et al. (2014) observed that with a larger fraction of precipitation occurring as rain instead of snow, the ratio of mean streamflow to mean precipitation generally is lower, possibly due to increased evapotranspiration in winter. Others have observed that with earlier snowmelt, the snowmelt rate tends to be slower, resulting in reduced snowmelt runoff (Barnhart, et all., 2016; Musselman et al., 2017). This is because reduced snowmelt rates result in larger partition to evapotranspiration, instead of subsurface or overland flow. However, there is a counteracting effect from vegetation water use that results in larger snowmelt runoff when it occurs earlier, because snowmelt occurs before the growing season, during which evapotranspiration is high (Barnhart, et al., 2020). The net effect of the above mechanisms is that climate-related changes in snowmelt runoff vary in different contexts, but overall, the relative contribution of snowmelt to total annual runoff is decreasing (Li, et al., 2017).

Aside from the timing and volume of snowmelt runoff, the shape of the spring snowmelt runoff pulse can be important for water management. Dust on snowpacks affects net radiation and therefore the energy balance of a snowpack (Painter, et al., 2010). As a result, years with higher dust concentrations tend to have steeper runoff pulses (Painter, et al., 2018). Because earlier snowmelt occurs at a time of year with less available radiation, a warmer climate arguably could reduce the peak value and average slope dust-related the runoff pulses (Barnhart, et al., 2016; Musselman, et al., 2017).

Among all the factors influencing snowmelt runoff, temperature is mostly commonly used to predict the timing, magnitude, and shape of snowmelt runoff pulse, due to the widespread availability of temperature observations. However, it has long been argued that including other variables could improve the performance of snowmelt runoff predictions (e.g., Zuzel & Cox, 1975). Historically, the degree-day approach has been widely used. In this approach, temperatures above zero are accumulated to reflect heat received by snowpack, and the result is used to predict snowmelt. The relatively simple Snowmelt Runoff Model (SRM) (Martinec, 1975; Rango & Martinec, 1979; Kustas, et al., 1994) is based on this approach. By incorporating net radiation received by the snowpacks as a predictor, the performance of SRM has been shown to be enhanced (Kustas, et al., 1994; Brubaker, et al., 1996; Hock, 1999; Vafakhah, et al., 2015). Arguably, radiation is as important as temperature (if not more so), because the energy balance controls the snowmelt process, and solar radiation (in most cases, especially in springtime) is the major energy source (Painter, et al., 2007). Net radiation is mainly influenced by cloud cover and snow albedo. In some regions, such as the southern Rocky Mountains in Colorado, dust on snow reduces the albedo, and is an important component of interannual variability (Painter, et al., 2012; Skiles, et al., 2015; Skiles, et al., 2018). Black carbon and organic carbon also contribute to this albedo reduction in some regions (Kaspari, et al., 2014; Zhang, et al., 2018). Reduction of snow albedo is likely to result in earlier snowmelt, and in some cases, reduction in total snowmelt runoff (Painter, et al, 2010; Painter, et al., 2018; Skiles, et al., 2018; Zhang, et al., 2018).

Due to lack of radiation observations, previous research on the relationship between radiation forcing and snowmelt runoff has been limited to well instrumented sites, for instance in Colorado (Painter, et al, 2010; Painter, et al., 2018; Fassnacht, et al., 2022). However, the Western United States contains various landscapes and climate types (Bales, et al., 2006; Trujillo & Molotch, 2014) which affect the space-time variations in net radiation. Here, this study extends the above studies to more sites across the Western United States and investigate the diversity of snowmelt runoff processes across the 20 sites across the Cascade Range, Sierra Nevada, the Rocky Mountains, Colorado Plateau, and the Great Basin.

This study used the Livneh daily CONUS near-surface gridded meteorological and derived hydrometeorological data (Livneh, et al., 2013). The Livneh dataset, which is at $1/16^{th}$ degree latitude-longitude spatial resolution across the conterminous U.S., provides a source of long-term meteorological forcings required to force large scale hydrological models. Net radiation in the Livneh data set is estimated using the Mountain Microclimate Simulation Model (MTCLIM; Thornton et al., 2000) algorithm. In the MTCLIM model, the only observed data is temperature (daily maximum and minimum) and precipitation. Downward solar radiation is estimated using the daily temperature range and vapor pressure. The reflectance is related to snow cover, slope, and vegetation type. The calculation of vapor pressure involves dew point (approximated by the daily minimum temperature with a correction for precipitation and net radiation). Because the calculation of vapor pressure and net radiation involves each other, an iteration is needed to approximate the result (Thornton et al., 2000). Bohn, et al. (2013) evaluated the performance of MTCLIM net radiation estimates globally, focusing on locations where short-wave radiation, long-wave radiation, and vapor pressure were all observed. Bohn et al. (2013) found that inland

sites have relatively unbiased estimates of short-wave radiation, compared with coastal sites. Estimates of long-wave radiation are relatively unbiased regardless of location. Because the sites chosen in our research all are inland in the sense used by Bohn et al. (2013), we argue that errors in the Livneh et al. (2013) net radiation should be modest.

2. Study Site and Datasets

2.1 Study Basins and Discharge Data

This study examined daily discharge data at 20 USGS sites. The sites span 10 states of the Western U.S.: Colorado, Utah, Wyoming, California, Nevada, Oregon, Washington, Arizona, Idaho, and Montana. The sites also span a range of hydroclimatic conditions. They lie within the northern Rocky Mountains, middle Rocky Mountains (Yellowstone region), southern Rocky Mountains, Sierra Nevada, The Cascade Range, Colorado Plateau, and Great Basin. All the sites have complete discharge records from water year 1985 on, and some have complete discharge records as far back as 1910. All the sites are free of anthropogenic influences, such as large reservoirs and diversions upstream of the gauges. Discharge data are daily mean values in cubic feet per second. The data were downloaded from the USGS National Water Information System: Web Interface (https://waterdata.usgs.gov/) in July 2022.

The drainage areas upstream of the USGS stream gauges were identified using Open Street Map (OSM) topographic map (Figure 2). The drainage basin areas range from 23 km^2 (#09047700) to 2154 km^2 (#13185000).

Figure 1. Location of the 20 selected USGS sites. The topographic base map was obtained from USGS National Water Information System: Map View (https://maps.waterdata.usgs.gov/).

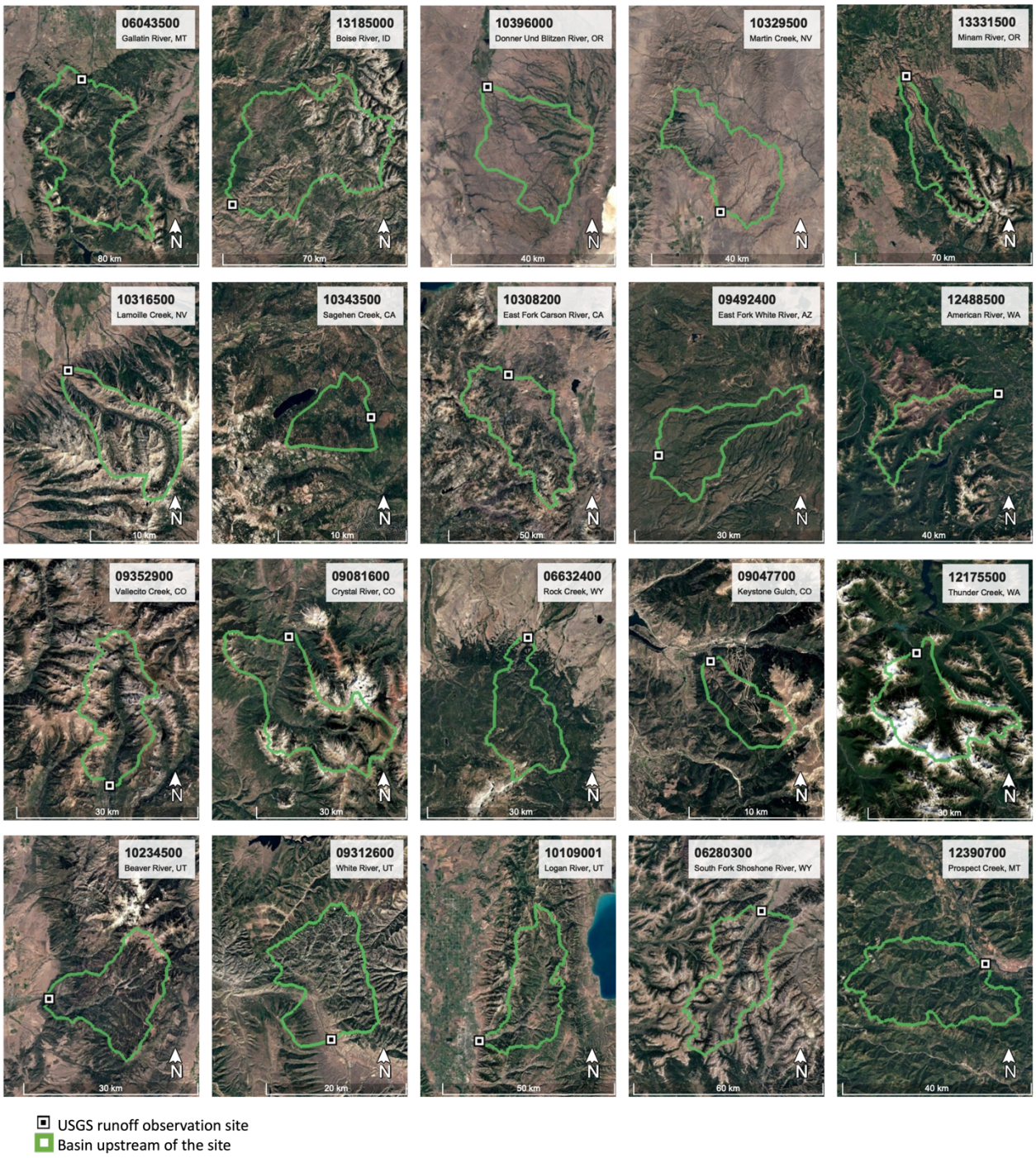

Figure 2. Satellite maps of selected gauges. Location of USGS gauges is shown by white squares with black centers. Basin boundaries upstream of gauges are shown with green lines. Scales (at lower right corner) are different for each map, depending on the basin area.

2.2 Radiation Data

One problem that has limited research on radiation forcings in the context of runoff is the lack of direct observations. A commonly used high quality radiation observation dataset, SURFRAD (Surface Radiation Budget) network, which has records since the 1990s, only has three stations in the Western U.S. Some research sites also exist, e.g., within the upper Colorado River Basin at the Senator Beck Basin, which is an independent research site rather than a widespread network (Painter et al., 2018; Fassnacht et al., 2022). As a practical matter, studies of the vast region of the Western U.S. have little choice but to use radiation data from model estimates, which can take various forms.

This study chose to use the radiation data from the Livneh daily conterminous U.S. (CONUS) near-surface gridded meteorological and derived hydrometeorological data (Livneh, et al., 2013). In the Livneh data set, the radiation-related variable is defined as the total amount of net longwave radiation and net shortwave radiation, which are both derived using the MTCLIM model introduced before. The resulting variable is net radiation. The spatial resolution of the Livneh dataset is 1/16th degree latitude-longitude, and the temporal resolution is 3-hour over the CONUS. We use the daily resolution instead of 3-hour resolution for the efficiency of calculation. Data are available for a 97-year period from January 1st, 1915, to December 31st, 2018. The part from October 1st, 1991 to September 30th, 2011 is chosen as the study period. The data were downloaded from the NOAA Physical Sciences Laboratory website (https://psl.noaa.gov/data/gridded/data.livneh.html).

2.3 Meteorological Data

Temperature, precipitation, and snow water equivalent are three meteorological and hydrological variables related to snowmelt runoff. Livneh dataset is also used as the source for these data. In the Livneh dataset, daily maximum temperature, daily minimum temperature, and daily precipitation are derived from observations at NOAA Cooperative Observer (COOP) stations. This station network, which includes about 20,000 stations, covers the CONUS. Daily snow water equivalent (SWE) in the Livneh data set is derived from the Variable Infiltration Capacity (VIC) model (Liang, et al., 1994) via energy budget closure. The VIC model generates hydrological and energy fluxes given the meteorological inputs. The spatial and temporal resolution and temporal coverage of these meteorological variables are the same as those for the radiation data (see Section 2.2). Considering the data coverage of our runoff data, radiation data, and meteorological data, we define a 20-year research period from water year 1992 to water year 2011.

3. Methods

3.1 Indices Describing Snowmelt Runoff Peak

This study used nine different indices to describe snowmelt runoff peaks: t_{Q25}, t_{Q50}, D_S, D_P, Q_S, Q_P, D_L, Q_L, and S (full names and definitions are listed in Table 1). The first four (t_{Q25}, t_{Q50}, D_S, and D_P) describe the timing of snowmelt runoff peaks. The fifth and sixth (Q_S and Q_P) describe

the magnitude of snowmelt runoff peaks. The last three (D_L, Q_L, and S) describe the shape of the rising limb of the hydrograph in the vicinity of snowmelt runoff peaks. We comment briefly below on the motivation and characteristics of the nine indices.

Table 1. Full name and definitions of the indices designed to describe snowmelt runoff peaks.

Indices	Full name	Definition
t_{Q25}	Time of 25% Runoff	The date when 25% of total water year runoff has occurred
t_{Q50}	Time of 50% Runoff	The date when 50% of total water year runoff has occurred
D_S	Start Date	The date when the snowmelt runoff peak starts
D_P	Peak Date	The date when the snowmelt runoff peak reaches its highest volume
Q_S	Start Runoff	The daily average runoff of Start Date
Q_P	Peak Runoff	The daily average runoff of Peak Date
D_L	Date Length	The number of days between Start Date and Peak Date
Q_L	Runoff Length	The difference between Start Runoff and Peak Runoff
S	Slope of Peak	The average slope of the snowmelt runoff peak

t_{Q25} and t_{Q50} represent the temporal distribution of runoff. t_{Q25} is the date when 25% of the total water year discharge has occurred. Similarly, t_{Q50} is the date when exactly 50% of the total water year discharge has occurred. t_{Q50} of an entire water year is equivalent to the center of timing (CT) for a water year, which is a commonly used index reflecting runoff distribution (Stewart, et al., 2004; Stewart, et al., 2005). Following Dudley, et al. (2017) and Fassnacht et al. (2022), t_{Q50} can be calculated for either a whole water year or a certain period, depending on the aim of the research. For example, t_{Q50} could be calculated over a period from January 1st to July 31st, or January 1st to September 30th, so that the influence of runoff peaks induced by autumn rainstorms is excluded from calculation. Here, considering that the normal starting time of snowmelt is always later than January, we calculate t_{Q25} and t_{Q50} over a period from February 1st

to July 31st. This period excludes the influence of autumn and early winter rainstorms. We define this period as the snowmelt season.

To describe the snowmelt runoff pulse more accurately, this study identified the start date (D_s) and peak date (D_P) of snowmelt runoff in each water year. The simplest definition of D_P is the day with the highest daily runoff during the snowmelt season. However, narrow peaks created by precipitation events can complicate the interpretation of D_P because these events occur randomly and do not necessarily represent real snowmelt runoff peaks. As a result, we redefined D_P as the day around which the total runoff in a 30-day period is the largest. The index thus is defined as:

D_P is n when $\sum_{i=n-15}^{n+15}(Q_i)$ is the maximum, in which n is the number of days since the start of water year, and Q_i is the daily average flow in the i^{th} day since start of water year. (365 should be 366 in leap years).

To restrict the result to the snowmelt season, we limit the range of n between 124 (Feb 1st) and 305 (Aug 1st). (305 should be 306 in leap years).

Identifying D_S is not as straightforward as identifying D_P. Cayan et al. (2001) first developed an algorithm that identified the onset of the snowmelt runoff pulse as the day when the cumulative departure from that year's mean flow is most negative. This is equivalent to identifying the day after which runoff is largely above average. This method works well for most high-elevation basins across the Western United States. Most research using this method adds a restriction to the occurrence time of the date, limiting the date to the snowmelt season, and excluding possible

high autumn runoff from rainfall (Cayan et al., 2001; Stewart, et al., 2005; Fritze, et al., 2011). Painter, et al. (2018) identify D_s as the date when deviation from the running mean flow since January 1st exceeds one percent. We compared the two methods, and decided to use the first one, since it captures the onset of streamflow peak more accurately, especially in basins with smaller peaks before the mean snowmelt peak. This method defines D_S as:

D_S is n when $\sum_{i=1}^{n}\left(Q_i - \frac{\sum_{j=1}^{365} Q_j}{365}\right)$ is the minimum, in which n is the number of days since the start of the water year, and Q_i, Q_j is the daily average flow in the i^{th} and j^{th} day since the start of the water year. (365 should be 366 in leap years).

To restrict the result to the snowmelt season, we limited the range of n between 124 (Feb 1st) and 305 (Aug 1st). (305 should be 306 in leap years).

Thus, a method to extract the runoff value of these two dates (Q_s and Q_P) from the daily runoff records is generated. $D_L = D_P - D_S$ is used to demonstrate the duration of the rising limb of the snowmelt runoff peak. $Q_L = Q_P - Q_S$ is used to demonstrate the magnitude of the snowmelt runoff peak. Finally, we can describe the rising limb of the snowmelt runoff pulse and calculate its average slope (S): $S = \frac{Q_L}{D_L} = \frac{Q_P - Q_S}{D_P - D_S}$.

The spatial distribution of average D_S, D_P, and Q_P are shown in Figure 3 (a-c). These three indices are typical indices for the timing and magnitude of snowmelt runoff, partly reflecting climate differences among sites. Because Q_P is proportional to the basin area, we further divide Q_P of each basin by area of the basin to generate a comparable amount. The spatial distribution

of Q_P/Area is shown in Figure 3 (d). D_S and D_P are influenced by both latitude and elevation. In general, sites in the Rockies and one site in the Cascade Range show later snowmelt than other sites. Q_P is largely influenced by basin area. Q_P/Area, which gets rid of this influence, generally reflects the humidity difference among sites. Sites in the Rockies, the Cascade Range, and Sierra Nevada generally show larger snowmelt runoff than sites in the Great Basin and Colorado Plateau. However, one Great Basin site (#10316500) has very large Q_P/Area value. This might be due to its small area and steep topology.

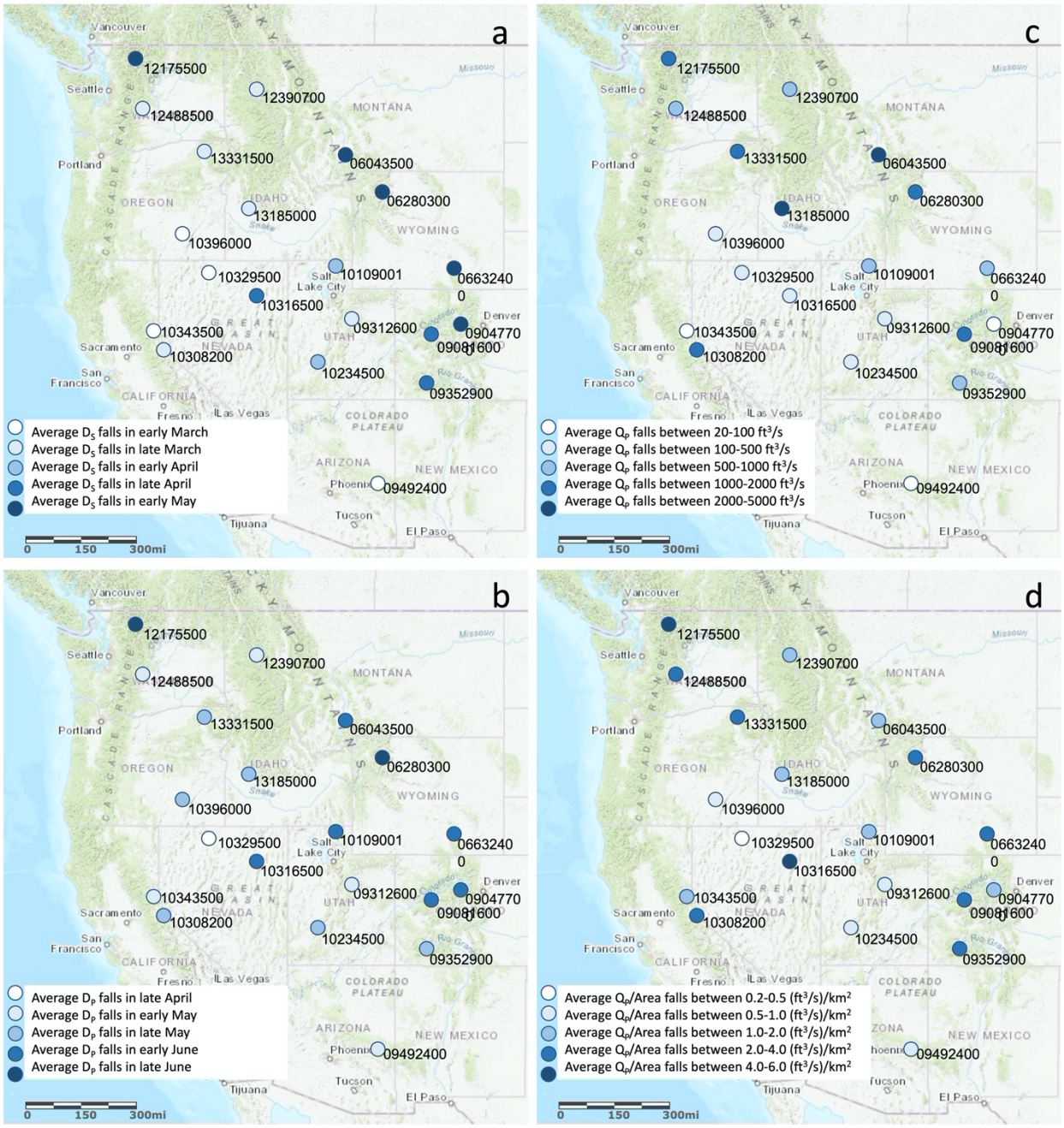

Figure 3. Spatial distribution of some of the indices and derived amount. They are (a) start date of snowmelt runoff (D_S), (b) peak date of snowmelt runoff (D_P), (c) peak runoff of snowmelt runoff (Q_P), and (d) peak runoff of snowmelt runoff divided by basin area (Q_P/Area). Color bar is used to show the magnitude of indices. Lighter colors are for smaller value, and darker colors are for larger value.

3.2 Radiation and Meteorology Variables

Radiation and meteorology variables from the Livneh dataset are 3-dimension arrays (x, y, and time). This study uses the river basin outlines to crop these data. If a part of a basin falls in a grid cell of the x-y array, it is defined as "inside" the basin. For net radiation, we noticed that the difference between snow albedo and bare ground albedo is the primary determining factor in the snowmelt season, when the snow coverage could vary over a short period and a small spatial scale. To bypass this disturbing factor, and to reflect the real yearly difference of net radiation over snow-covered surface (which might relate to dust deposition in snow), we calculated the average daily radiation energy of the snow-covered area during the melt season. We first identified the last snow-covered date of each cell in each year from the SWE data of Livneh dataset. Then, we calculated the average net radiation for each cell over the melting period, which is from the average snowmelt start date to the last snow-covered date. The average snowmelt start date is the yearly average of D_S (start date of snowmelt runoff, defined in section 3.1) of the given site. Finally, we calculated a weighted average of the result of different grid cells. The weight is proportional to the number of days between average snowmelt start date and last snow-covered date (which varies among cells and years). The defined index is abbreviated as Q_{net}.

Then, considering that even for the meteorology variables, whose value is not as strongly related to snowpack as net radiation, cells with more snowpack are more important in our analysis, this study calculates a weight for each cell that is proportional to its total SWE over the research period (1992-2011). This weight is used to calculate a weighted mean value of meteorology variables for each basin. This method ensures that the cells with largest snow cover are considered more.

All the cells inside a basin are averaged to generate values for that basin: for any meteorology variable V of a basin at any time t, $V_{basin,t} = \sum_{j=1}^{n} w_j V_{j,t}$, in which n is the number of cells inside the basin, w_j is the weight of the jth cell, and $V_{j,t}$ is the variable value of the jth cell at time t. Thus, for each variable, a 2-demension array (20 basin and 20-year of daily value) is generated. This method might include some parts (slightly) outside the basin, but this is acceptable and necessary, because some of the smallest basins are smaller than the cell size (about 30 km^2) and averaging more cells around it should reduce random errors. However, to do comparison between years, it is necessary to calculate some indexes reflecting the average intensity of radiation and meteorological forcings of each year. The basic thought is to average the daily values together, but we need to carefully consider the period over which the data are averaged. The detailed calculation of indices is introduced in the following paragraphs. The full names and definitions of defined variables are listed in Table 2.

Table 2. Full name and definitions of the indices designed to reflect average magnitude of radiation and meteorology forcings.

Indices	Full name	Definition
Q_{net}	Average net radiation	Average daily net radiation energy over snow-covered area during melting season (from average snowmelt runoff start date to last snow-covered date)
T_{maxW}	Average maximum temperature of winter	Average maximum temperature from January 1st to average snowmelt runoff start date
T_{minW}	Average minimum temperature of winter	Average minimum temperature from January 1st to average snowmelt runoff start date
$Prec_W$	Average precipitation of winter	Average precipitation from January 1st to average snowmelt runoff start date
T_{maxS}	Average maximum temperature of spring	Average maximum temperature from average snowmelt runoff start date to average snowmelt runoff peak date
T_{minS}	Average minimum temperature of spring	Average minimum temperature from average snowmelt runoff start date to average snowmelt runoff peak date
$Prec_S$	Average precipitation of spring	Average precipitation from average snowmelt runoff start date to average snowmelt runoff peak date

SWE	Maximum SWE of water year	Maximum SWE from October 1st to average snowmelt runoff peak date of the same water year

For maximum temperature, minimum temperature, and precipitation, two different indexes are calculated for each variable, reflecting winter and spring average, respectively. In particular, the winter average is defined as an average before snowmelt, while the spring average is defined as an average during the snowmelt process. Because snowmelt occurs at different time in different basins, it is necessary to calculate a unique time range for each site separately. We used two indices defined in section 3.1 to capture the timing of snowmelt. They are the start date (D_S) and peak date (D_P) of snowmelt runoff. Then, we averaged D_S and D_P over the research period (1992-2011) for each basin (see Figure 3), to generate a typical season landmark regardless of annual variations. We calculated the average of maximum temperature, minimum temperature, and precipitation between January 1st and average D_S to generate the winter average of each variable (T_{maxW}, T_{minW}, and $Prec_W$). We calculated the average of maximum temperature, minimum temperature, and precipitation between average D_S and average D_P to generate the spring average of each variable (T_{maxS}, T_{minS}, and $Prec_S$).

For SWE, the maximum SWE of the whole snow season (October 1st to average D_P) is used to represent the relative magnitude of snow precipitation of a water year. This index is also abbreviated as SWE, since it's the only SWE related index regardless of season.

3.3 Correlation Analysis of variables

This study used Pearson's correlation coefficient and the corresponding p-values to identify relationships between X variables (radiation and meteorology variables) and Y variables (indices describing the snowmelt runoff peak). It used eight X variables (Q_{net}, T_{maxW}, T_{maxS} T_{minW}, T_{minS}, $Prec_W$, $Prec_S$, and SWE) and nine Y variables (t_{Q25}, t_{Q50}, D_S, D_P, Q_S, Q_P, D_L, Q_L, and S) in total. So, there are 72 pairs of relationships for each of the 20 sites. For each single site, then, we can determine the major factors determining the features of snowmelt runoff peak, and the directions and strength of the interactions. Obviously, any X variable is not independent with other X variables, which is also true for any Y variable. Thus, we also perform similar correlation analyses between different X variables and between different Y variables, generating 28 pairs of relationships between X variables and 36 pairs of relationships between Y variables. We classified the correlation results by the P-value. We defined P-value<0.05 as the threshold for significant correlations. We defined P-value<0.0001 as the threshold for very significant correlations. Then, for each variable pair, we counted the number of sites with very significant positive correlation, significant positive correlation, non-significant correlation, significant negative correlation, and very significant correlation. These five numbers could reflect the general relationship between two variables. For variable pairs that we want to investigate more, we would list the specific sites that show some kinds of correlation and map the sites to check if any spatial pattern exists.

4. Results

4.1 Correlation between Snowmelt Runoff Indices

This study first analyzed the relationships between snowmelt runoff indices. The results are displayed in Table 3. Among all the variable pairs, some show significant positive correlations at most sites (>15), and very significant positive correlations at part of the sites (>5). They are D_S - D_P, D_S - t_{Q25}, D_S - t_{Q50}, Q_S - Q_P, D_P - t_{Q25}, D_P - t_{Q50}, Q_S - Q_P, Q_S - Q_L, Q_S - S, Q_P - Q_L, Q_P - S, Q_P - t_{Q25}, Q_P - t_{Q50}, Q_L - S, Q_L - t_{Q25}, and t_{Q25} - t_{Q50}. We conclude that the timing indices of snowmelt runoff (D_S, D_P, t_{Q25}, and t_{Q50}) are highly related. This is because the snowmelt runoff is the largest runoff event in the year, and thus determines the timing of t_{Q25} and t_{Q50}. Also, the time difference between D_S and D_P, which is defined as D_L, is irrelevant with other timing indices. As a result, whenever D_S is earlier, D_P is also earlier. They change in the same direction. Another conclusion is that the slope of the snowmelt runoff peak is solely determined by the magnitude of snowmelt runoff, which is reflected in the variable Q_L. Moreover, Q_L is highly related with Q_S and Q_P, which also show positive correlation between themselves. That means the four related variables, S, Q_L, Q_S, and Q_P, all reflect the annual variance of snowmelt magnitude. There doesn't exist such events as low but steep runoff peaks, or runoff peaks starting low and ending high. We also found that t_{Q25} and t_{Q50} are highly correlated with Q_P and Q_L, but D_S and D_P don't show this relationship. This is because the calculation of t_{Q25} and t_{Q50} also involves the proportion of snowmelt runoff to total runoff.

Table 3. Results of Pearson correlation coefficient analysis for Y variable pairs (pairs of indices designed to describe snowmelt runoff peaks). For each variable pair, the results of 20 sites are classified according to the sign of correlation coefficient (positive and negative) and the magnitude of P-value (<0.0001 as very significant, <0.05 as significant, and >0.05 as non-significant). For non-significant results, the sign of correlation coefficient is not distinguished. The first column shows the variable pairs in their abbreviations (see Table 1 for full names and definitions). Note that the number of sites in the very significant column is also included in the significant column.

Variable Pair	Positive and very significant P-value<0.0001	Positive and significant P-value<0.05	Non-significant P-value>0.05	Negative and significant P-value<0.05	Negative and very significant P-value<0.0001

$D_S - D_P$	5	16	4	0	0
$D_S - Q_S$	1	13	7	0	0
$D_S - Q_P$	1	16	4	0	0
$D_S - D_L$	0	0	10	10	3
$D_S - Q_L$	1	14	6	0	0
$D_S - S$	2	16	4	0	0
$D_S - t_{Q25}$	12	19	1	0	0
$D_S - t_{Q50}$	5	18	2	0	0
$D_P - Q_S$	0	12	8	0	0
$D_P - Q_P$	0	17	3	0	0
$D_P - D_L$	2	9	11	0	0
$D_P - Q_L$	1	17	3	0	0
$D_P - S$	0	6	13	1	1
$D_P - t_{Q25}$	9	15	5	0	0
$D_P - t_{Q50}$	14	17	3	0	0
$Q_S - Q_P$	16	20	0	0	0
$Q_S - D_L$	0	1	17	2	0
$Q_S - Q_L$	14	18	2	0	0
$Q_S - S$	6	18	2	0	0
$Q_S - t_{Q25}$	4	14	6	0	0
$Q_S - t_{Q50}$	2	16	4	0	0
$Q_P - D_L$	0	1	16	3	0
$Q_P - Q_L$	20	20	0	0	0
$Q_P - S$	13	19	1	0	0
$Q_P - t_{Q25}$	9	17	3	0	0
$Q_P - t_{Q50}$	5	17	3	0	0
$D_L - Q_L$	0	2	15	3	0
$D_L - S$	0	0	9	11	1
$D_L - t_{Q25}$	0	1	16	3	0
$D_L - t_{Q50}$	0	2	17	1	0
$Q_L - S$	14	19	1	0	0
$Q_L - t_{Q25}$	8	17	3	0	0
$Q_L - t_{Q50}$	4	18	2	0	0
$S - t_{Q25}$	2	15	5	0	0
$S - t_{Q50}$	0	9	11	0	0
$t_{Q25} - t_{Q50}$	18	20	0	0	0

Then, there are variable pairs that show a dominant direction (>5, with the other direction <5) of correlation, but with less significant and very significant sites. The pairs with dominant positive correlation include D_S - Q_S, D_S - Q_P, D_S - Q_L, D_S - S, D_P - Q_S, D_P - Q_P, D_P - D_L, D_P - Q_L, D_P - S, Q_S - t_{Q25}, Q_S - t_{Q50}, Q_L - t_{Q50}, Q_L - t_{Q50}, and S - t_{Q50}. Pairs with dominant negative correlation include D_S - D_L and D_L - S. The two pairs with dominant negative correlation and some of the pairs with dominant positive correlation are merely a result of the calculation method (e.g., D_L = D_P - D_S). Some other pairs reflect a correlation between the timing and magnitude of snowmelt runoff peak. These correlations are dominantly positive, indicating that earlier snowmelt runoff tends to be smaller in magnitude.

The rest of the variable pairs are mostly non-significant and doesn't have a dominant direction. They are Q_S - D_L, Q_P - D_L, D_L - Q_L, D_L - t_{Q25}, and D_L - t_{Q50}. Obviously, D_L is a special index, which is relatively independent with other indices.

4.2 Correlation between Radiation and Meteorological Forcings

Then, relationships between radiation and meteorological forcing variables are analyzed. For most variable pairs, non-significant correlations are dominant (>15). These pairs include Q_{net} - T_{maxW}, Q_{net} - T_{minW}, Q_{net} - $Prec_W$, Q_{net} - SWE, T_{maxW} - T_{maxS}, T_{maxW} - T_{minS}, T_{maxW} - $Prec_S$, T_{maxS} - T_{minW}, T_{maxS} - $Prec_W$, T_{minW} - $Prec_W$, T_{minW} - $Prec_S$, T_{minW} - SWE, T_{minS} - $Prec_W$, T_{minS} - $Prec_S$, T_{minS} - SWE, and $Prec_W$ - $Prec_S$. These include the relationship between Q_{net} and all the winter-related variables. This means that net radiation of melting season is relatively independent with weather conditions of winter. We also noticed that, in most cases, temperature and precipitation

forcings are usually independent between different seasons (e.g., T_{maxW} - T_{maxS}). Minimum temperature is not relevant with any of the precipitation and SWE variables, but maximum temperature is relevant with the precipitation of the corresponding season, as well as SWE.

Table 4. Results of Pearson correlation coefficient analysis for X variable pairs (pairs of indices reflecting radiation and meteorology variables). For each variable pair, the results of 20 sites are classified according to the sign of correlation coefficient (positive and negative) and the magnitude of P-value (<0.0001 as very significant, <0.05 as significant, and >0.05 as non-significant). For non-significant results, the sign of correlation coefficient is not distinguished. The first column shows the variable pairs in their abbreviations (see Table 1 for full names and definitions). Note that the number of sites in the very significant column is also included in the significant column.

Variable Pair	Positive and very significant P-value<0.0001	Positive and significant P-value<0.05	Non-significant P-value>0.05	Negative and significant P-value<0.05	Negative and very significant P-value<0.0001
$Q_{net} - T_{maxW}$	0	0	19	1	0
$Q_{net} - T_{maxS}$	6	18	2	0	0
$Q_{net} - T_{minW}$	0	0	19	1	0
$Q_{net} - T_{minS}$	1	8	12	0	0
$Q_{net} - Prec_W$	0	2	18	0	0
$Q_{net} - Prec_S$	0	0	9	11	0
$Q_{net} - SWE$	0	4	16	0	0
$T_{maxW} - T_{maxS}$	0	2	18	0	0
$T_{maxW} - T_{minW}$	12	18	2	0	0
$T_{maxW} - T_{minS}$	0	4	16	0	0
$T_{maxW} - Prec_W$	0	0	12	8	0
$T_{maxW} - Prec_S$	0	0	20	0	0
$T_{maxW} - SWE$	0	0	7	13	0
$T_{maxS} - T_{minW}$	0	2	17	1	0
$T_{maxS} - T_{minS}$	6	17	3	0	0
$T_{maxS} - Prec_W$	0	0	16	4	0
$T_{maxS} - Prec_S$	0	0	3	17	5
$T_{maxS} - SWE$	0``	0	12	8	1
$T_{minW} - T_{minS}$	0	6	13	1	0
$T_{minW} - Prec_W$	0	1	19	0	0
$T_{minW} - Prec_S$	0	0	20	0	0
$T_{minW} - SWE$	0	0	19	1	0

T_{minS} – $Prec_W$	0	0	18	2	0
T_{minS} – $Prec_S$	0	0	20	0	0
T_{minS} – SWE	0	0	16	4	0
$Prec_W$ – $Prec_S$	0	4	16	0	0
$Prec_W$ – SWE	12	20	0	0	0
$Prec_S$ – SWE	1	8	12	0	0

Some variable pairs show significant correlation of same sign in most sites (>15), and very significant correlation in part of sites (>5). The variable pairs with positive correlation include Q_{net} - T_{maxS}, T_{maxW} - T_{minW}, T_{maxS} - T_{minS}, and $Prec_W$ - SWE. The variable pairs with negative correlation include T_{maxS} - $Prec_S$. We found that net radiation of the melting season is positively correlated with average maximum temperature of the same period. This is because both variables are associated with clear sky conditions. Despite the different degree of influence that precipitation has on maximum and minimum temperatures (see previous paragraph), maximum and minimum temperature changes synchronously in the same season. $Prec_W$ and SWE are related because winter precipitation falls mostly in the form of snow at all the sites. One important observation is that the average maximum temperature of spring is negatively correlated with spring precipitation in most sites. This is because precipitation is associated with cloud cover which is associated with relatively cool conditions.

Finally, some variable pairs do not have a dominant (>15) correlation type. They are Q_{net} - T_{minS}, Q_{net} - $Prec_S$, T_{maxW} - $Prec_W$, T_{maxS} - SWE, T_{maxW} - SWE, T_{minW} - T_{minS}, and $Prec_S$ - SWE. We map the sites with different correlation results in Figure 4 (a-g). Sites with significant negative correlation between Q_{net} and T_{minS} or $Prec_S$ (Figure 4 (a, b)) are similar. They are sites with relatively later snowmelt runoff (see Figure 3 (a, b)), which means lower temperature and longer snow cover. Thus, the difference between years with clear conditions and more snowy conditions

is more stably reflected in the variation of net radiation. Sites with significant negative correlation between T_{maxW} and $Prec_W$ or SWE (Figure 4 (c, e)) are similar. They are mostly sites in the northeastern side, where the cloudiness of winter could lower maximum temperature. Sites with significant negative correlation between T_{maxS} and SWE, as well as significant positive correlation between $Prec_S$ and SWE (Figure 4 (d, g)) are mostly the same. They are sites in the southern side of the research region, where maximum SWE could occur in spring, and thus relate to the spring precipitation and temperature. The spatial distribution of the sites with correlation between T_{minW} and T_{minS} is harder to explain. The possible reason for a positive correlation between them is the continuous influence of snow cover on temperature. Otherwise, temperature of winter and spring shouldn't be correlated with each other.

Figure 4. Distribution of sites with different correlation results for variable pairs with no dominant correlation type (>15 sites). They are (a) Q_{net} - T_{minS}, (b) Q_{net} - $Prec_S$, (c) T_{maxW} - $Prec_W$, (d) T_{maxS} - SWE, (e) T_{maxW} - SWE, (f) T_{minW} - T_{minS}, (g) $Prec_S$ - SWE. Blue points are used for sites with significant (P-value<0.05) negative correlations, and red points are used for sites with significant (P-value<0.05) positive correlations. White points are used for sites with non-significant correlations (P-value>0.05).

4.3 Correlation between Radiation and Snowmelt Runoff Indices

Then, this study analyzed the correlation between Q_{net} and the snowmelt runoff indices (D_S, D_P, Q_S, Q_P, D_L, Q_L, S, t_{Q25}, and t_{Q50}). Results are shown in Table 5. For many of the sites, the correlations between Q_{net} and Q_S, Q_P, Q_L, D_L, or S are non-significant. For many of the sites, the negative correlations between Q_{net} and t_{Q25} or t_{Q50} are significant. About half of the sites show significant negative correlation between Q_{net} and D_S or D_P. In general, the relationship between net radiation and the timing of snowmelt runoff is stronger than that between net radiation and the magnitude of the snowmelt runoff. We list the detailed correlation results of each site with significant in Table 6. We will interpret the results in the next paragraphs and map these sites in Figure 5.

Table 5. Results of Pearson correlation coefficient analysis for Q_{net} and snowmelt runoff indices. For each variable pair, the results of 20 sites are classified according to the sign of correlation coefficient (positive and negative) and the magnitude of P-value (<0.0001 as very significant, <0.05 as significant, and >0.05 as non-significant). For non-significant results, the sign of correlation coefficient is not distinguished. The first column shows the variable pairs in their abbreviations (see Table 1 for full names and definitions). Note that the number of sites in the very significant column is also included in the significant column.

Variable Pair	Positive, P-value<0.0001	Positive, P-value<0.05	Non-significant	Negative, P-value<0.05	Negative, P-value<0.0001
$Q_{net} - D_S$	0	0	11	9	0
$Q_{net} - D_P$	0	0	9	11	2
$Q_{net} - Q_S$	0	2	13	5	0
$Q_{net} - Q_P$	0	1	13	6	0
$Q_{net} - D_L$	0	1	18	1	0
$Q_{net} - Q_L$	0	0	15	5	0
$Q_{net} - S$	0	0	19	1	0
$Q_{net} - t_{Q25}$	0	0	4	16	2
$Q_{net} - t_{Q50}$	0	0	7	13	1

Table 6. Results of Pearson correlation coefficient analysis for each site. Signs in the cells show positive or negative correlation significance. Blank cells show non-significant correlation. Sites with non-significant correlation are not shown

Site ID	Q_{net} - D_S	Q_{net} - D_P	Q_{net} - Q_S	Q_{net} - Q_P	Q_{net} - D_L	Q_{net} - Q_L	Q_{net} - S	Q_{net} - t_{Q25}	Q_{net} - t_{Q50}
09352900									
09081600								-	
10234500	-	-	-	-		-		-	-
06632400	-	-	-	-		-	-	-	-
10308200								-	
10316500	-	-	-	-		-		-	-
06280300	-	-			-			-	-
10343500		-						-	-
10396000			-	-		-		-	-
10109001	-	-						-	-
09492400			+	+					
13185000	-								-
09047700	-	-		-	+	-		-	-
06043500	-	-						-	-
09312600		-	-	-				-	-
10329500								-	-
13331500								-	
12488500	-	-						-	
12390700			+					-	
12175500		-							-

Most sites show significant negative correlation between Q_{net} and at least one of t_{Q25} and t_{Q50}. This means when net radiation is larger, the timing of runoff tends to be earlier. Only two sites are exceptions: site #09352900 and site #09492400. Both sites are in the southernmost part of our study region. These two sites differ in that Q_{net} shows no significant correlation with any indices at site #09352900, while Q_{net} shows significant positive correlation with snowmelt magnitude indices (Q_S and Q_P) at site #09492400. However, this positive correlation is caused by the calculation method of Q_{net}. In years with low snow (which could happen in such warm sites

as site #09492400), the last snow-covered date could occur before the average start date of snowmelt. Thus, the result of Q_{net} is zero. Site #09492400 is the only site where this kind of exception occurs and causes a false positive correlation between Q_{net} and snowmelt magnitude (which is positively correlated with snow fall amount). In general, in these two warmest sites, net radiation is not related with snowmelt runoff.

Whenever there is significant negative correlation between Q_{net} and Q_L or S, there is significant negative correlation between Q_{net} and Q_P. The strong relationship between these three indices has been explained in section 4.1. D_L is relatively random and the correlation between it and Q_{net} could be negative or positive, depending on the how D_S and D_P is sensitive to Q_{net} variation. However, it is for sure that both D_S and D_P are negatively correlated with Q_{net} (if significant). Finally, we decided to focus on the pattern of D_S, D_P, Q_S, and Q_P. We simply refer to D_S and D_P as timing indices and refer to Q_S and Q_P as magnitude indices. The two timing indices always show similar results with each other because they are positively correlated at most sites. This is also true for the two magnitude indices. We can classify all the sites into four groups based on if Q_{net} is negatively correlated with any of the timing or magnitude indices (Table 7). We also map the four groups in Figure 5.

Table 7. Sites classified into four groups based on whether Q_{net} is negatively correlated with timing indices (D_S and D_P) and magnitude indices (Q_S and Q_P).

significant negative correlation between Q_{net} and any of the timing indices	**significant negative correlation between Q_{net} and any of the magnitude indices**	**Sites that apply**
Yes	Yes	#10234500, #06632400, #10316500, #09047700, #09312600,
Yes	No	#06280300, #10343500, #10109001, #13185000, #06043500, #12488500, #12175500
No	Yes	#10396000,

No	No	#09081600, #10308200, #10329500, #13331500, #12390700, #09352900, #09492400

Only one site belongs to the third group, in which Q_{net} shows negative correlation with magnitude indices only. This means that the negative correlation between Q_{net} and timing indices is more common than that between Q_{net} and magnitude indices. In general, whenever there is negative correlation between Q_{net} and magnitude indices, there is also negative correlation between Q_{net} and timing indices. There are five sites that show negative correlation between Q_{net} and both timing and magnitude indices (the first group). There are seven sites that show negative correlation between Q_{net} and timing indices only (the second group). These two groups have very clear spatial patterns. In general, the first group is located in the southeastern part of our study region, including the Great Basin and the Colorado Rockies. The second group is located in the northeastern and northwestern part of our study region, including Sierra Nevada, the Cascades, and northern Rockies. This difference could possibly relate to different climate types. In the southeastern part of our study region, precipitation is lower than in the northeastern and northwestern parts. Lower precipitation means larger sensitivity of snowpack to radiation forcings. Finally, there are seven sites where Q_{net} shows no significant correlation with any of the indices. They have no clear spatial pattern.

Figure 5. Distribution of four types of sites, classified by the correlation results between Q_{net} and snowmelt runoff indices. Grey points show sites with negative correlation between Q_{net} and both timing (D_S and D_P) and magnitude indices (Q_S and Q_P). Orange points show sites with negative correlation between Q_{net} and timing indices only. Blue points show sites with negative correlation between Q_{net} and magnitude indices only. White points show sites with no significant negative correlation between Q_{net} and any of the timing and magnitude indices

4.4 Correlation between Meteorology variables and Snowmelt Runoff Indices

This study first calculated the correlation between temperature related variables and snowmelt runoff indices. The results are listed in Table 8. In almost all the cases, the correlation between temperature and snowmelt indices is negative (if significant). Thus, we conclude that with higher temperature (no matter in winter or spring, and no matter maximum or minimum temperature), snowmelt runoff tends to be earlier and smaller. Then, we noticed that the correlation between

maximum temperature and snowmelt runoff indices is stronger than that between minimum temperature and snowmelt runoff indices. The correlation between spring temperature and snowmelt runoff indices is stronger than that between winter temperature and snowmelt runoff indices. Then, we investigated the details and found several variable pairs that most sites (>15) show significant negative correlation. They are T_{maxS} - D_P, T_{maxS} - Q_P, T_{maxS} - Q_L, T_{maxS} - t_{Q25}, T_{maxS} - t_{Q50}, and T_{minS} - t_{Q50}. Obviously, average maximum temperature of spring is the best predictor of snowmelt runoff. Whenever this index is higher, we expect an earlier and smaller snowmelt runoff.

Table 8. Results of Pearson correlation coefficient analysis for temperature related variables (T_{maxW}, T_{maxS}, T_{minW}, and T_{minS}) and snowmelt runoff indices. For each variable pair, the results of 20 sites are classified according to the sign of correlation coefficient (positive and negative) and the magnitude of P-value (<0.0001 as very significant, <0.05 as significant, and >0.05 as non-significant). For non-significant results, the sign of correlation coefficient is not distinguished. The first column shows the variable pairs in their abbreviations (see Table 1 for full names and definitions). Note that the number of sites in the very significant column is also included in the significant column.

Variable Pair	Positive, P-value<0.0001	Positive, P-value<0.05	Non-significant	Negative, P-value<0.05	Negative, P-value<0.0001
$T_{maxW} - D_S$	0	0	15	5	0
$T_{maxW} - D_P$	0	0	16	4	0
$T_{maxW} - Q_S$	0	0	13	7	0
$T_{maxW} - Q_P$	0	0	11	9	0
$T_{maxW} - D_L$	0	0	20	0	0
$T_{maxW} - Q_L$	0	0	12	8	0
$T_{maxW} - S$	0	0	14	6	0
$T_{maxW} - t_{Q25}$	0	0	13	7	1
$T_{maxW} - t_{Q50}$	0	0	16	4	0
$T_{maxS} - D_S$	0	0	7	13	1
$T_{maxS} - D_P$	0	0	4	16	10
$T_{maxS} - Q_S$	0	0	11	9	0
$T_{maxS} - Q_P$	0	0	2	18	2
$T_{maxS} - D_L$	0	0	16	4	0
$T_{maxS} - Q_L$	0	0	2	18	2

$T_{maxS} - S$	0	0	13	7	0
$T_{maxS} - t_{Q25}$	0	0	3	17	8
$T_{maxS} - t_{Q50}$	0	0	1	19	14
$T_{minW} - D_S$	0	1	16	3	0
$T_{minW} - D_P$	0	0	20	0	0
$T_{minW} - Q_S$	0	0	20	0	0
$T_{minW} - Q_P$	0	0	17	3	0
$T_{minW} - D_L$	0	1	19	0	0
$T_{minW} - Q_L$	0	0	17	3	0
$T_{minW} - S$	0	0	19	1	0
$T_{minW} - t_{Q25}$	0	0	19	1	0
$T_{minW} - t_{Q50}$	0	0	20	0	0
$T_{minS} - D_S$	0	0	12	8	0
$T_{minS} - D_P$	0	0	7	13	2
$T_{minS} - Q_S$	0	0	17	3	0
$T_{minS} - Q_P$	0	0	16	4	0
$T_{minS} - D_L$	0	0	18	2	0
$T_{minS} - Q_L$	0	0	16	4	0
$T_{minS} - S$	0	0	19	1	0
$T_{minS} - t_{Q25}$	0	0	9	11	0
$T_{minS} - t_{Q50}$	0	0	3	17	3

The predictivity of temperature related indices among different sites is compared by counting the total number of variable pairs that show significant negative correlation for each site. The result is shown in Figure 6. The distribution of number is clustered. There are 2 sites within 5-6, 12 sites within 8-11, 1 site of 15, and five sites within 18-21. Their spatial distribution is also clustered. Sites with the 18-21 significant variable pairs generally locate in the northeastern and northwestern side of the research region. Sites with 8-11 significant variable pairs generally locate in the middle and southern side of the research region. The rest three sites with 5-6 or 15 significant variable pairs are not clustered. We investigate the difference between two larger

clusters and found that the 18-21 group differs from the 8-11 group in that their winter temperature show stronger correlation with snowmelt runoff indices.

Figure 6. Spatial distribution of the number of variable pairs that show significant negative correlation between temperature related variables and snowmelt runoff indices. Color bar is used to show the number. Lighter colors are for smaller value, and darker colors are for larger value. The division of color bar is designed according to the clustered distribution of the results.

Next, this study calculated the correlation between precipitation and SWE related variables and snowmelt runoff indices. The results are listed in Table 9. In almost all the cases, the correlation between precipitation and SWE related and snowmelt indices is positive (if significant). Thus, we conclude that with higher precipitation and SWE (no matter in winter or spring), snowmelt runoff tends to be later and larger. For brevity, we simply define the predictivity of a X variable for a Y variable as the number of sites that show significant positive correlation between X and

Y and compare the three X variables. For D_S and D_P, SWE is the best predictor, slightly better than $Prec_S$. Both are better than $Prec_W$. For Q_S, Q_P, Q_L, and S, SWE is the best predictor, slightly better than $Prec_W$. Both are better than $Prec_S$. For t_Q25 and t_Q50, $Prec_S$ is the best predictor, slightly better than SWE. Both are better than $Prec_W$. For D_L, none of the variables could predict well. In general, SWE, which largely depends on winter precipitation, determines the magnitude of snowmelt runoff (which is a way stronger relationship than that between temperature, net radiation and snowmelt runoff magnitude). In contrast, spring precipitation is more related with the timing of snowmelt runoff. There are several ways spring precipitation might influence snowmelt timing. First, more cloud cover could lower temperature, net radiation, and as a result, energy balance of snowpack. Second, spring precipitation that falls as snow in the high-elevation part of the basin could increase average albedo and reduce net radiation of the period after snow, thus reducing energy balance. Third, the additive snow itself could prolong the snowmelt process and put peak runoff toward a later date.

Table 9. Results of Pearson correlation coefficient analysis for precipitation and SWE related variables ($Prec_W$, $Prec_S$, and SWE) and snowmelt runoff indices. For each variable pair, the results of 20 sites are classified according to the sign of correlation coefficient (positive and negative) and the magnitude of P-value (<0.0001 as very significant, <0.05 as significant, and >0.05 as non-significant). For non-significant results, the sign of correlation coefficient is not distinguished. The first column shows the variable pairs in their abbreviations (see Table 1 for full names and definitions). Note that the number of sites in the very significant column is also included in the significant column.

Variable Pair	Positive, P-value<0.0001	Positive, P-value<0.05	Non-significant	Negative, P-value<0.05	Negative, P-value<0.0001
PrecW – DS	0	4	16	0	0
PrecW – DP	0	5	15	0	0
PrecW – QS	2	16	4	0	0
PrecW – QP	3	18	2	0	0
PrecW – DL	0	1	18	1	0
PrecW – QL	2	15	5	0	0
PrecW – S	1	8	12	0	0

PrecW – tQ25	0	8	12	0	0
PrecW – tQ50	1	7	13	0	0
PrecS – DS	0	7	13	0	0
PrecS – DP	0	11	9	0	0
PrecS – QS	0	9	11	0	0
PrecS – QP	0	10	10	0	0
PrecS – DL	0	3	17	0	0
PrecS – QL	0	9	11	0	0
PrecS – S	0	4	16	0	0
PrecS – tQ25	0	12	8	0	0
PrecS – tQ50	0	13	7	0	0
SWE – DS	0	8	12	0	0
SWE – DP	0	10	10	0	0
SWE – QS	9	18	2	0	0
SWE – QP	13	20	0	0	0
SWE – DL	0	2	16	2	0
SWE – QL	11	19	1	0	0
SWE – S	2	12	8	0	0
SWE – tQ25	2	10	10	0	0
SWE – tQ50	1	12	8	0	0

Like what is done for temperature related variables, this study also put all precipitation and SWE related variables together and count the number of significant variable pairs for each site. The results are shown in Figure 7. The distribution of number is less clustered than the results of temperature related variables. The spatial pattern shows more smooth transition between sites with more significant variable pairs and sites with less significant variable pairs. Sites where precipitation and SWE related variables show higher predictivity for snowmelt runoff locate in the Rockies and Sierra Nevada. Sites in the northwestern side of the research region show poorer predictivity.

Figure 7. Spatial distribution of the number of variable pairs that show significant positive correlation between precipitation and SWE related variables and snowmelt runoff indices. Color bar is used to show the number. Lighter colors are for smaller value, and darker colors are for larger value. The division of color bar is designed according to the clustered distribution of the results.

5. Discussion and Conclusions

This paper investigated how various forcing factors determine the timing and magnitude of snowmelt runoff peaks in 20 river basins distributed across the Western U.S. First, we sought a group of indices that describes variations in the magnitude and timing of snowmelt runoff peaks across the stations. It is found that the onset and peak of snowmelt runoff vary synchronously, and they determine the temporal distribution of runoff in the snowmelt season, since snowmelt runoff is the predominant runoff event in this period. On the other hand, the period between the onset of snowmelt runoff and its peak, the length of the rising limb, doesn't show any clear

relationship with other variables, indicating that earlier or later snowmelt doesn't necessarily correspond to a shorter or longer rising limb of the runoff peak. As for the magnitude indices, we found that runoff at the onset of snowmelt varies synchronously with peak runoff, notwithstanding that peak runoff is much higher. As a result, the runoff difference between onset and peak almost equals peak runoff, although it is also positively correlated with onset runoff. Since yearly variations of peak runoff are much larger than that of the period between onset date and peak date, the slope of the rising limb is also determined by the magnitude of peak runoff, making it a key index. We expected to find relatively independent indices in at least three dimensions that describe runoff peaks: timing, magnitude, and shape. However, the shape index is highly correlated with the magnitude index, leaving only two dimensions. Moreover, there is a weak but significant positive correlation between the timing of peak runoff and its magnitude; in particular, earlier runoff peaks are usually smaller than the later ones.

This paper subsequently investigated several factors that have been proposed as influencing snowmelt runoff features. They are net radiation (winter), temperature (winter and spring), precipitation (winter and spring), and SWE (maximum). We first look into the relationships between these factors. A large proportion of the variables we chose are independent with each other, but some variable pairs show higher correlations. Some are because they are related inherently. These include the relationship between maximum and minimum temperature and between winter precipitation and SWE. Some others are due to physical mechanisms, which we are most interested in. These include the relationship between maximum temperature and precipitation (as well as SWE), between net radiation and spring temperature and spring precipitation, and between winter temperature and spring temperature. Some of the relationships

only occur in part of the sites. However, considering that the correlation are of the same sign if significant, they reflect similar relationship in most cases, which only differ in magnitude of correlation.

The main conclusion of this paper comes from the correlation analysis between influencing factors and the snowmelt runoff indices. We first investigated the correlation between net radiation and snowmelt. Net radiation is negatively correlated with timing of runoff in most sites. In other words, in years with higher net radiation, snowmelt runoff tends to occur earlier. At a few sites (concentrated around the Great Basin and Colorado Rockies), net radiation is negatively correlated with the magnitude of snowmelt runoff. This might be an artifact of our method of calculating the net radiation index. For each grid cell, net radiation is averaged over a period with snow cover. Thus, in years with later snowmelt, a grid cell could receive more net radiation later in the melt season, when the incidence angle is larger. This could cause a bias toward larger net radiation, and result in a false positive correlation between our net radiation index and snowmelt timing if there's no actual correlation between them. However, because we found negative correlation between net radiation and snowmelt timing, we conclude that this bias does not impact our conclusion.

Temperature is negatively correlated to the timing and magnitude of snowmelt runoff, though the predictivity of temperature varies by site. In general, maximum temperature and spring temperature are more correlated with snowmelt runoff indices than minimum temperature and winter temperature. Some sites in the northeastern and northwestern side of our research region are more sensitive to temperature. They differ from other sites in that winter temperature is also

related to snowmelt runoff. These sites are clustered in high-latitude regions, but we haven't found plausible physical mechanism behind it. Precipitation and SWE are positively correlated to the timing and magnitude of snowmelt runoff, though the predictivity also varies by site. Maximum SWE is the best indicator for the magnitude of snowmelt runoff among all factors and does well in predicting the timing of snowmelt runoff. Spring precipitation is more correlated with the timing of snowmelt runoff, while winter precipitation is more correlated with the magnitude of snowmelt runoff. Sites in the Rockies and Sierra Nevada are more sensitive to precipitation and SWE factors than other sites. Northwestern sites are especially not sensitive to precipitation and SWE factors. In general, the finding agrees with previous research; snowmelt runoff tends to be earlier and smaller with higher temperature, or with lower precipitation (or SWE).

References

Adam, J. C., Hamlet, A. F., & Lettenmaier, D. P. (2008). Implications of global climate change for snowmelt hydrology in the twenty-first century. *Hydrological Processes*, 23(7), 962-972. https://doi.org/10.1002/hyp.7201

Bales, R. C., Molotch, N. P., Painter, T. H., Dettinger, M. D., Rice, R., & Dozier, J. (2006). Mountain hydrology of the western United States. *Water Resources Research*, 42(8). https://doi.org/10.1029/2005WR004387

Barnett, T. P., Adam, J. C., & Lettenmaier, D. P. (2005). Potential impacts of a warming climate on water availability in snow-dominated regions. *Nature*, 438, 303-309. https://doi.org/10.1038/nature04141

Barnhart, T. B., Molotch, N. P., Livneh, B., Harpold, A. A., Knowles, J. F., & Schneider, D. (2016). Snowmelt rate dictates streamflow. *Geophysical Research Letters*, 43(15), 8006-8016. https://doi.org/10.1002/2016GL069690

Barnhart, T. B., Tague, C. L., & Molotch, N. P. (2020). The counteracting effects of snowmelt rate and timing on runoff. *Water Resources Research*, 56(8). https://doi.org/10.1029/2019WR026634

Berghuijs, W. R., Woods, R. A., & Hrachowitz, M. (2014). A precipitation shift from snow towards rain leads to a decrease in streamflow. *Nature Climate Change*, 4(7), 583-586. https://doi.org/10.1038/nclimate2246

Bohn, T. J., Livneh, B., Oyler, J. W., Running, S. W., Nijssen, B., & Lettenmaier, D. P. (2013). Global evaluation of MTCLIM and related algorithms for forcing of ecological and hydrological models. *Agricultural and Forest Meteorology*, 176, 38-49. https://doi.org/10.1016/j.agrformet.2013.03.003

Brubaker, K., Rango, A., & Kustas, W. (1996). Incorporating radiation inputs into the snowmelt runoff model. *Hydrological processes*, 10(10), 1329-1343. https://doi.org/10.1002/(SICI)1099-1085(199610)10:10<1329::AID-HYP464>3.0.CO;2-W

Cayan, D. R., Kammerdiener, S. A., Dettinger, M. D., Caprio, J. M., & Peterson, D. H. (2001). Changes in the onset of spring in the western United States. *Bulletin of the American Meteorological Society,* 82(3), 399-416. https://doi.org/10.1175/1520-0477(2001)082<0399:CITOOS>2.3.CO;2

Cho, E., McCrary, R. R., & Jacobs, J. M. (2021). Future Changes in Snowpack, Snowmelt, and Runoff Potential Extremes Over North America. *Geophysical Research Letters*, 48(22). https://doi.org/10.1029/2021GL094985

Clow, D. W. (2010). Changes in the timing of snowmelt and streamflow in Colorado: a response to recent warming. *Journal of Climate*, 23(9), 2293-2306.

Davenport, F. V., Herrera-Estrada, J. E., Burke, M., & Diffenbaugh, N. S. (2020). Flood size increases nonlinearly across the western United States in response to lower snow-precipitation ratios. Water Resources Research, 56(1). https://doi.org/10.1029/2019WR025571

Dudley, R. W., Hodgkins, G. A., McHale, M. R., Kolian, M. J., & Renard, B. (2017). Trends in snowmelt-related streamflow timing in the conterminous United States. *Journal of Hydrology*, 547, 208-221. https://doi.org/10.1016/j.jhydrol.2017.01.051

Earman, S., Campbell, A. R., Phillips, F. M., & Newman, B. D. (2006). Isotope exchange between snow and atmospheric water vapor: Estimation of the snowmelt component of groundwater recharge in the southwestern United States. *Journal of Geophysical Research: Atmospheres*, 111(D9). https://doi.org/10.1029/2005JD006470

Fassnacht, S. R., Duncan, C. R., Pfohl, A. K. D., Webb, R. W., Derry, J. E., Sanford, W. E., Reimanis, D. C., & Doskocil, L. G. (2022). Drivers of dust-enhanced snowpack melt-out and streamflow timing. *Hydrology*, 9(3), 47. https://doi.org/10.3390/hydrology9030047

Fritze, H., Stewart, I. T., & Pebesma, E. (2011). Shifts in western North American snowmelt runoff regimes for the recent warm decades. *Journal of Hydrometeorology*, 12(5), 989-1006. https://doi.org/10.1175/2011JHM1360.1

Hamlet, A. F., Mote, P. W., Clark, M. P., & Lettenmaier, D. P. (2005). Effects of temperature and precipitation variability on snowpack trends in the western United States. *Journal of Climate*, 18(21), 4545-4561. https://doi.org/10.1175/JCLI3538.1

Hock, R. (1999). A distributed temperature-index ice-and snowmelt model including potential direct solar radiation. *Journal of Glaciology*, 45(149), 101-111. https://doi.org/10.3189/S0022143000003087

Kaspari, S., Painter, T. H., Gysel, M., Skiles, S. M., & Schwikowski, M. (2014). Seasonal and elevational variations of black carbon and dust in snow and ice in the Solu-Khumbu, Nepal and estimated radiative forcings. *Atmospheric Chemistry and Physics*, 14(15), 8089-8103. https://doi.org/10.5194/acp-14-8089-2014

Kustas, W. P., Rango, A., & Uijlenhoet, R. (1994). A simple energy budget algorithm for the snowmelt runoff model. *Water Resources Research*, 30(5), 1515-1527. https://doi.org/10.1029/94WR00152

Li, D., Wrzesien, M. L., Durand, M., Adam, J., & Lettenmaier, D. P. (2017). How much runoff originates as snow in the western United States, and how will that change in the future? *Geophysical Research Letters*, 44(12), 6163-6172. https://doi.org/10.1002/2017GL073551

Liang, X., Lettenmaier, D. P., Wood, E. F., & Burges, S. J. (1994). A simple hydrologically based model of land surface water and energy fluxes for general circulation models. *Journal of Geophysical Research: Atmospheres*, 99(D7), 14415-14428. https://doi.org/10.1029/94JD00483

Livneh, B., Rosenberg, E. A., Lin, C., Nijssen, B., Mishra, V., Andreadis, K. M., Maurer, E. P., & Lettenmaier, D. P. (2013). A long-term hydrologically based dataset of land surface fluxes and states for the conterminous United States: Update and extensions. *Journal of Climate*, 26(23), 9384-9392. https://doi.org/10.1175/JCLI-D-12-00508.1

Mankin, J. S., Viviroli, D., Singh, D., Hoekstra, A. Y., & Diffenbaugh, N. S. (2015). The potential for snow to supply human water demand in the present and future. *Environmental Research Letters*, 10(11), 114016. https://doi.org/10.1088/1748-9326/10/11/114016

Martinec, J. (1975). Snowmelt-runoff model for stream flow forecasts. *Hydrology Research*, 6(3), 145-154. https://doi.org/10.2166/nh.1975.0010

McCabe, G. J. & Clark, M. P. (2005). Trends and variability in snowmelt runoff in the western United States. *Journal of Hydrometeorology*, 6(4), 476-482. https://doi.org/10.1175/JHM428.1

Mote, P. W., Hamlet, A. F., Clark, M. P., & Lettenmaier, D. P. (2005). Declining mountain snowpack in western North America. *Bulletin of the American meteorological Society*, 86(1), 39-50. https://doi.org/10.1175/BAMS-86-1-39

Musselman, K. N., Clark, M. P., Liu, C., Ikeda, K., & Rasmussen, R. (2017). Slower snowmelt in a warmer world. *Nature Climate Change*, 7(3), 214-219. https://doi.org/10.1038/nclimate3225

Painter, T. H., Barrett, A. P., Landry, C. C., Neff, J. C., Cassidy, M. P., Lawrence, C. R., ... & Farmer, G. L. (2007). Impact of disturbed desert soils on duration of mountain snow cover. *Geophysical Research Letters*, 34(12). https://doi.org/10.1029/2007GL030284

Painter, T. H., Deems, J. S., Belnap, J., Hamlet, A. F., Landry, C. C., & Udall, B. (2010). Response of Colorado River runoff to dust radiative forcing in snow. *Proceedings of the National Academy of Sciences*, 107(40), 17125-17130. https://doi.org/10.1073/pnas.0913139107

Painter, T. H., Skiles, S. M., Deems, J. S., Bryant, A. C., & Landry, C. C. (2012). Dust radiative forcing in snow of the Upper Colorado River Basin: 1. A 6 year record of energy balance, radiation, and dust concentrations. *Water Resources Research*, 48(7). https://doi.org/10.1029/2012WR011985

Painter, T. H., Skiles, S. M., Deems, J. S., Brandt, W. T., & Dozier, J. (2018). Variation in rising limb of Colorado River snowmelt runoff hydrograph controlled by dust radiative forcing in snow. *Geophysical Research Letters*, 45(2), 797-808. https://doi.org/10.1002/2017GL075826

Qin, Y., Abatzoglou, J. T., Siebert, S., Huning, L. S., Aghakouchak, A., Mankin, J. S., Hong, C., Tong, D., Davis, S. J., & Mueller, N. D. (2020). Agricultural risks from changing snowmelt. *Nature Climate Change*, 10(5), 459-465. https://doi.org/10.1038/s41558-020-0746-8

Rango, A., & Martinec, J. (1979). Application of a snowmelt-runoff model using Landsat data. *Hydrology Research*, 10(4), 225-238. https://doi.org/10.2166/nh.1979.0006

Skiles, S. M., Mallia, D. V., Hallar, A. G., Lin, J. C., Lambert, A., Petersen, R., & Clark, S. (2018). Implications of a shrinking Great Salt Lake for dust on snow deposition in the Wasatch Mountains, UT, as informed by a source to sink case study from the 13–14 April 2017 dust event. *Environmental Research Letters*, 13(12), 124031. https://doi.org/10.1088/1748-9326/aaefd8

Skiles, S. M., Painter, T. H., Belnap, J., Holland, L., Reynolds, R. L., Goldstein, H. L., & Lin, J. (2015). Regional variability in dust-on-snow processes and impacts in the Upper Colorado River Basin. *Hydrological Processes*, 29(26), 5397-5413. https://doi.org/10.1002/hyp.10569

Stewart, I. T. (2008). Changes in snowpack and snowmelt runoff for key mountain regions. *Hydrological Processes*, 23(1), 78-94. https://doi.org/10.1002/hyp.7128

Stewart, I. T., Cayan, D. R., & Dettinger, M. D. (2004). Changes in snowmelt runoff timing in western north america under a "business as usual" climate change scenario. *Climate Change*, 62, 217-232. https://doi.org/10.1023/B:CLIM.0000013702.22656.e8

Stewart, I. T., Cayan, D. R., & Dettinger, M. D. (2005). Changes toward earlier streamflow timing across western North America. *Journal of climate*, 18(8), 1136-1155. https://doi.org/10.1175/JCLI3321.1

Thornton, P. E., Hasenauer, H., & White, M. A. (2000). Simultaneous estimation of daily solar radiation and humidity from observed temperature and precipitation: An application over complex terrain in Austria. *Agriculture and Forest Meteorology*, 104, 255–271, https://doi.org/10.1016/S0168-1923(00)00170-2

Trujillo, E., & Molotch, N. P. (2014). Snowpack regimes of the western United States. *Water Resources Research,* 50(7), 5611-5623. https://doi.org/10.1002/2013WR014753

Uzun, S., Tanir, T., Coelho, G. D. A., Souza de Lima, A. D., Cassalho, F., & Ferreira, C. M. (2021). Changes in snowmelt runoff timing in the contiguous United States. *Hydrological Processes*, 35(11), e14430. https://doi.org/10.1002/hyp.14430

Vafakhah, M., Nouri, A., & Alavipanah, S. K. (2015). Snowmelt-runoff estimation using radiation SRM model in Taleghan watershed. *Environmental Earth Sciences*, 73(3), 993-1003. https://doi.org/10.1007/s12665-014-3449-5

Wang, R., Kumar, M., & Link, T. E. (2016). Potential trends in snowmelt-generated peak streamflows in a warming climate. *Geophysical Research Letters*, 43(10), 5052-5059. https://doi.org/10.1002/2016GL068935

Westerling, A. L., Hidalgo, H. G., Cayan, D. R., & Swetnam, T. W. (2006). Warming and earlier spring increase western US forest wildfire activity. *Science*, 313(5789), 940-943. https://doi.org/10.1126/science.1128834

Zhang, Y., Kang, S., Sprenger, M., Cong, Z., Gao, T., Li, C., Tao, S., Li, X., Zhong, X., Xu, M., Meng, W., Neupane, B., Qin, X., & Sillanpää, M. (2018). Black carbon and mineral dust in snow cover on the Tibetan Plateau. *The Cryosphere*, 12(2), 413-431. https://doi.org/10.5194/tc-12-413-2018

Zuzel, J. F., & Cox, L. M. (1975). Relative importance of meteorological variables in snowmelt. *Water Resources Research*, 11(1), 174-176. https://doi.org/10.1029/WR011i001p00174